iScience

CellPress
OPEN ACCESS

Article

Terahertz exposure enhances neuronal synaptic transmission and oligodendrocyte differentiation *in vitro*

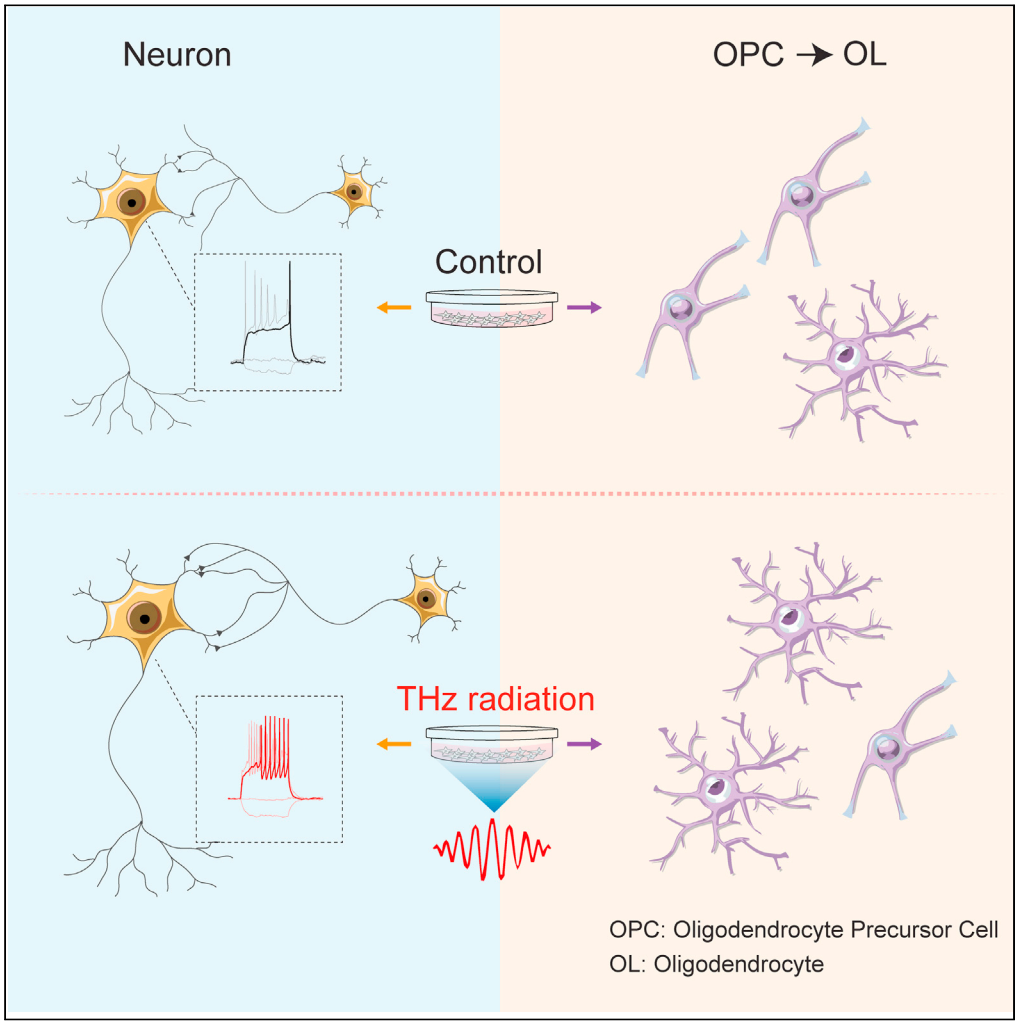

Xianghui Zhao, Ming Zhang, Yuming Liu, ..., Na Zhi, Wenting Wang, Shengxi Wu

wwt0657@fmmu.edu.cn (W.W.)
shengxi@fmmu.edu.cn (S.W.)

Highlights

THz irradiation increases excitatory synaptic transmission and neuronal firing

Microarray assay reveals neuronal gene expression dynamics after THz exposure

THz irradiation promotes the maturation of oligodendrocytes

The myelination process in neuron is enhanced after THz exposure

Zhao et al., iScience 24, 103485
December 17, 2021
https://doi.org/10.1016/j.isci.2021.103485

iScience

CellPress
OPEN ACCESS

Article

Terahertz exposure enhances neuronal synaptic transmission and oligodendrocyte differentiation *in vitro*

Xianghui Zhao,[1,3] Ming Zhang,[1,3] Yuming Liu,[1,3] Haiying Liu,[1] Keke Ren,[1] Qian Xue,[1] Haifeng Zhang,[1] Na Zhi,[1,2] Wenting Wang,[1,4,*] and Shengxi Wu[1,*]

SUMMARY

Terahertz (THz) frequency occupies a large portion of the electromagnetic spectrum that is between the infrared and microwave regions. Recent advances in THz application have stimulated interests regarding the biological effects within this frequency range. In the current study, we report that irradiation with a single-frequency THz laser on mice cortical neuron cultures increases excitatory synaptic transmission and neuronal firing activities. Microarray assay reveals gene expression dynamics after THz exposure, which is consistent with morphology and electrophysiology results. Besides, certain schedule of THz irradiation inhibits the proliferation of oligodendrocyte precursor cells (OPCs) and promotes OPC differentiation. Of note, the myelination process is enhanced after THz exposure. In summary, our observations suggest that THz irradiation can modulate the functions of different neuronal cells, with different sensitivity to THz. These results provide important understanding of the mechanisms that govern THz interactions with nervous systems and suggest THz wave as a new strategy for neuromodulation.

INTRODUCTION

In recent years, widespread applications of terahertz (THz) in security, military, and medical imaging have promoted increasing scientific interest in the biological effects associated with this frequency range. The THz region is typically defined to include the frequencies ranging from 0.1 to 10 THz, which occupies a large portion of the electromagnetic spectrum that is located between the infrared and microwave regions. For the effective development of diagnostic and therapeutic techniques, it is essential to be aware of fundamental biological effects of THz radiation.

Several studies using different THz sources and irradiance incident have tested THz bioeffects on living animals or cell cultures. As to the nervous system, early study showed that rat or mice receiving THz exposures may develop increased levels of depression and anxiety (Bondar et al., 2008; Kirichuk et al., 2009). But the detailed mechanism is unclear. Olshevskaya et al. observed that THz radiation caused injury to the morphology of neurons in a power- and wavelength-dependent manner (Olshevskaya et al., 2009). Transparent blank protrusions of the membrane, disorders of neurite growth, and fall of the membrane potential were observed in their study. Meanwhile, there are also negative results in the study of the biological effects of THz radiation. Bourne et al. indicated no effects of THz radiation on the differentiation or cell viability of ND7/23 cell line, with characteristics of sensory neurons, at a frequency of 0.14 THz or a power of 0.45 J/cm^2 (Bourne et al., 2008).

Considering the characteristics of the THz wave, especially that THz photons possess very low energies and have low penetration in water, we believe a well-controlled environmental setup is necessary for the study of the THz effect on cell cultures, which might be an explanation for discrepancies in previous studies. In the current study, we set up a THz exposure chamber with controlled temperature and CO_2 concentration and humidity, which guarantee the consistent environment for cell cultures during irradiation. We investigated the effect of THz irradiation on two types of cells, cortical neurons and oligodendrocytes; the latter is responsible for myelin formation on axons in the central nervous system (Nave and Werner, 2014). In particular, we used a single-frequency continuous wave laser source, 3.1 THz, a frequency band that efficiently

[1]Department of Neurobiology, School of Basic Medicine, Fourth Military Medical University, Xi'an, Shaanxi 710032, China

[2]College of Life Sciences, Northwest University, Xi'an, Shaanxi 710127, China

[3]These authors contributed equally

[4]Lead contact

*Correspondence: wwt0657@fmmu.edu.cn (W.W.), shengxi@fmmu.edu.cn (S.W.)

https://doi.org/10.1016/j.isci.2021.103485

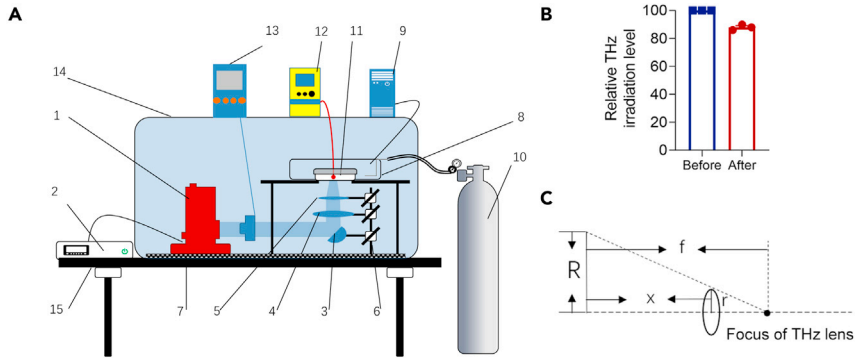

Figure 1. Setup of a temperature-controlled THz exposure chamber

(A) Schematic representation of the experimental setups. 1) THz QCL with stainless steel base, 2) CW/QCW current source, 3) OPA, 4) THz mirror, 5) THz lens, 6) support rod for optic mirror, 7) optical breadboard, 8) thermal controlled chamber, 9) heater controller, 10) mixed gas unit, 11) cell culture dish, 12) digital thermometer with 80PK-1 bead probe thermocouples, 13) THz sensor connected to THz power meter, and 14) shock-proof operating platform.

(B) Quantification of the relative THz irradiation level with (After) or without (Before) the culture dish. Data are mean ± SEM relative to "Before" from three independent measurements.

(C) Formula for calculating the height of culture dish (x) according to the defined spot area. R is defined as the radius of the THz lens (R = 12.7 mm), f is the effective focus length (f = 50 mm), and r is the radius of the defined spot area (r = 5 mm in our study).

See also Figures S1 and S2.

interacts with biomolecules important for cellular activity, such as water, amino acids, nucleobases, and glucose (Romanenko et al., 2017; Smye et al., 2001), to irradiate cell cultures for 15 min/three times/day or 3 h/one time/day. After several days' irradiation, neurons were analyzed for the expression of neurite outgrowth and synaptic-associated genes and the electrophysiological functions. Microarray assay was used to identify transcriptome alterations after THz exposure. For oligodendrocytes, we tested cell proliferation, differentiation, and myelination with qRT-PCR and immunostaining assay. In the current study, we found no significant temperature increase during THz irradiation; correspondingly, the expression levels of previously reported genes reflecting thermal mechanisms, e.g., heat shock proteins, were practically unaffected. These results indicate that our observations reveal non-thermal effects of THz on neuronal cultures.

RESULTS

The environmental controlled exposure conditions ensure the non-thermal and non-cytotoxic effect of THz on cell cultures

To achieve high-quality *in vitro* THz biological studies, we used a temperature-controlled exposure chamber (Figure 1A). The stainless steel chamber is designed for living cell imaging and consists of a stage heater and condenser aperture cover heater with a temperature controller. High humidity levels are maintained through a circular, heated water tank equipped with carbon dioxide injectors fed by a remote gas-mixing unit (5% CO_2, 95% air). We tested THz power on the sample stage, with or without the confocal dish, and found that the dish with polymer coverslip showed low absorption for THz power (Figure 1B). In addition, we recorded THz power after 3 h irradiation, which is the same as the power at the beginning (Figure S1A). Therefore, these results ensure consistent THz exposure in attached cells during 3 h.

To detect the possible temperature fluctuation during THz exposure, we recorded the temperature of the dish surface with or without THz irradiation in the preliminary experiment. With fast response and laboratory accuracy (0.05% + 0.3°C) characteristic, the thermometer connected to a dish cover with TSU-200F Thermo Probe did not reveal significant temperature rise during 3-h exposure to THz radiation (Figure S1B) (the control group varies from 35.08 to 35.18°C; THz group varies from 34.98 to 35.23°C; RMANOVA, n = 4 for each group, $F_{\text{within group}}$ (2.561,17.93) = 0.8593, p = 0.4648; $F_{\text{between group}}$ (1,6) = 0.02413, p = 0.8816).

In addition, before we test the possible function of THz exposure on neuron cultures, we examined potential cytotoxic effects by patch-clamp recording and TUNEL assay (terminal deoxynucleotidyl transferase dUTP nick end labeling). With long-term irradiation protocols as introduced in the methods, neuron cultures irradiated with THz for successive days showed normal action potential overshoot and frequent

spontaneous postsynaptic events (Figure S2A). Besides, the irradiated neurons did not show significantly increased numbers of TUNEL positive apoptotic cells (Figures S2B and S2C). Oligodendrocytes irradiated with the same protocol also revealed similar results of TUNEL staining with neurons culture (Figures S2B and S2D). Also, we examined the mRNA expression of *Hsp40* and *Hsp70* by quantitative RT-PCR assay, which are representative genes for minimal stress. All these genes did not show significant changes after THz exposure (Figure S2E). Together, these observations indicated there is no obvious effect of 3.1 THz on cell survival in current conditions.

THz exposure promotes neurite outgrowth and increases the expression of synaptic-associated proteins

Then we tested the neurite outgrowth and synaptogenesis after THz irradiation by examining the expression of neurite and synaptic genes. Since neurite outgrowth and synaptic development increase quickly during early neuronal development, neurons were irradiated from 2 days *in vitro* (2 DIV) to 5 DIV and tested at 6 DIV by immunostaining and qRT-PCR assay (Figure 2A). After 4-day irradiation, neuron cultures at low density ($2 \times 10^4/cm^2$) from short-term THz exposure (15 min, 3 times a day, with 3-h intervals between each irradiation) were collected. Quantitative RT-PCR revealed the significant upregulation of neurite outgrowth genes, *Tuj1* and *Gap43*, as well as synaptic genes, *Homer1* and *Synapsin* (*Syn*), in THz-irradiated cultures (Figures 2B and 2C). Besides, immunocytochemistry with antibodies against Homer1, a post-synaptic protein, and Tuj1 showed increased percentage of $Homer1^+$ cells among $Tuj1^+$ cells in the THz group, compared with the control group (Figures 2D and 2E).

To further confirm the enhanced synaptogenesis in neurons exposed to THz, we examined neuron cultures at higher density ($10^5/cm^2$), in which cells contact each other more easily. In the immunocytochemistry study, we noticed that there were increased numbers of $Homer1^+$ immunoreactive spots along $Tuj1^+$ neurites in higher-density cultures, indicating the formation of synapse between neurons (Figure 2F). Quantification of the number of immunoreactive spots by Imaris software revealed the increased $Homer1^+$ spots density after THz exposure (Figure 2G). In addition, western blot assay indicated the upregulation of synaptic protein, Synaptophysin (Syn), in THz-irradiated culture samples at both 4 and 6 DIV (Figure 2H). Similar results were observed in long-term irradiation protocols (cultures were irradiated for 3 h, one time a day, data not shown). Together, these observations suggest that THz irradiation can promote neurite outgrowth and enhance the establishment of synapses in neuron cultures.

THz irradiation enhances the excitatory synaptic transmissions and neuronal activities

To investigate the functional consequences of THz irradiation on synapses, we performed whole-cell patch clamp recording on cultured neurons. Since only the fully matured neurons can be used for electrophysiology study, neurons were irradiated from 5 to 9 DIV and tested at 12 DIV for electrophysiology activity. We first compared the neuronal activity-dependent spontaneous excitatory synaptic transmissions between the THz group and the control group. We found the average frequency of spontaneous excitatory synaptic currents (sEPSCs) was significantly higher in the THz group than in the control group (Figures 3A and 3B). The cumulative frequency distribution curve of sEPSCs' interevent interval in the THz group also was shifted left compared with the control group (Figure 3C). The average amplitudes of sEPSCs were similar between the THz group and control group (Figures 3A and 3D). However, the cumulative distribution curve of sEPSCs' amplitude in the THz group was moved right compared with the control group, suggesting that the amplitude of sEPSCs was increased in the THz group (Figure 3E). To test whether the receptor mechanisms involved in the sEPSCs change in THz radiation, we compared the rising and decay slope of sEPSCs between the control and THz radiation groups. We did not find any difference between these two groups (Figure S3). Moreover, we noticed that both the control group and THz group showed rhythmic synchronized big events during the sEPSCs recording (Figure 3F). In the THz group, the interval of these synchronized events was significantly reduced compared with those in the control group (Figure 3G). The area of these two groups did not show significant difference (Figure 3H). These results suggest that THz irradiation promotes excitatory synaptic transmissions.

Neurons rely on the action potential (AP) to deliver information from integrating the synapses and cell body, and the neurite outgrowth also needs the action potential to send growth information. So next we tested the neuronal intrinsic properties and firing rate in these two groups. There are two types of firing modes of the recorded neurons in our culture condition, the delay firing mode neurons (DFNs, Figure 4A) and the regular firing mode neurons (RFNs, Figure S4A). DFNs often started firing at the end of stimulation when the current injection reached rheobase. RFNs could generate AP at the early stage of the stimulation

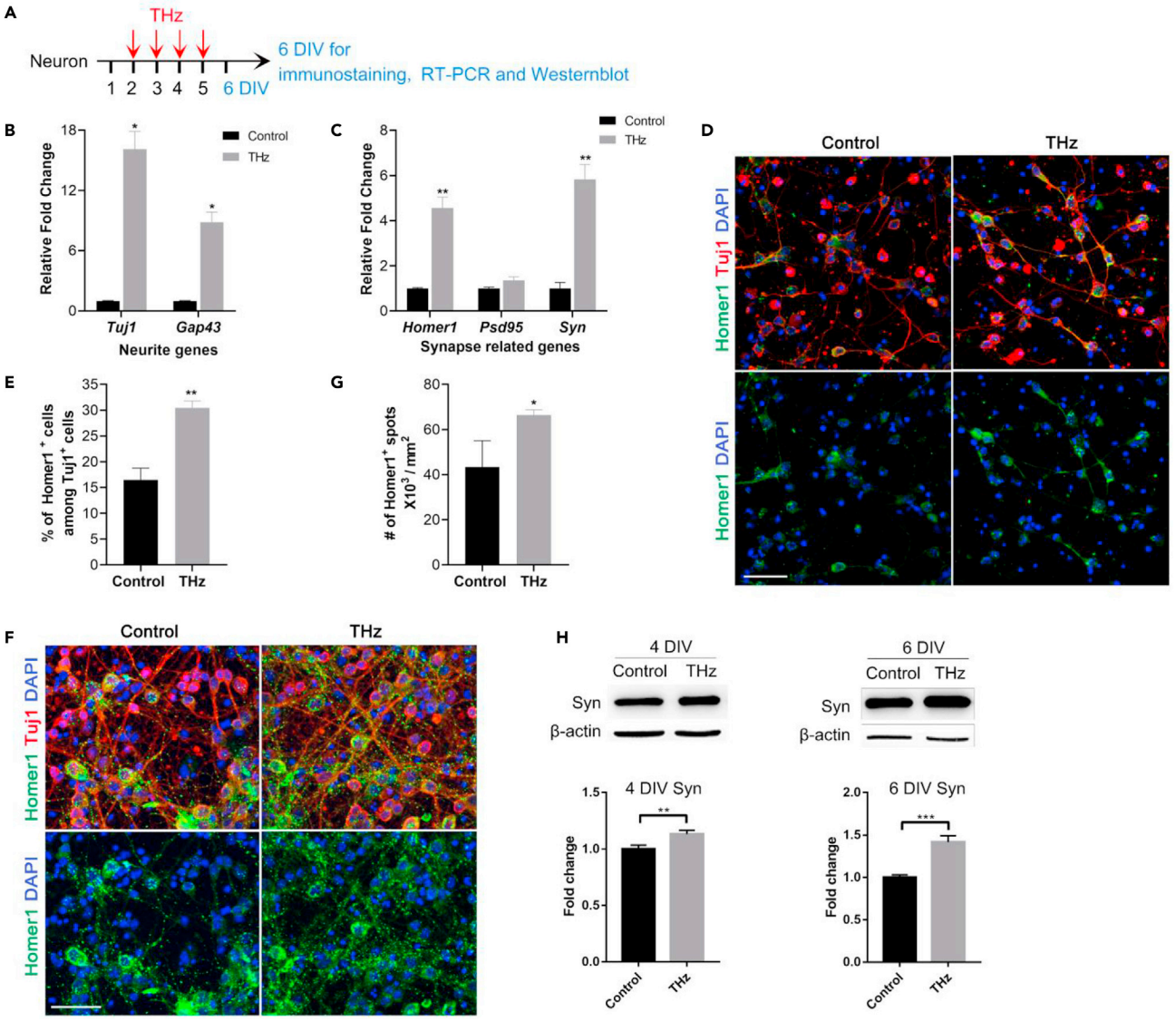

Figure 2. THz exposure promotes neurite outgrowth and synaptogenesis

(A) Diagram showing THz irradiation and succeeding analysis on neurons.

(B) Quantitative real-time PCR for neurite growth genes, *Tuj1* and *Gap43*, in THz-irradiated low-density neurons and control cultures. Data are mean ± SEM of transcript levels relative to control after normalization from three independent experiments each performed in triplicate. *p < 0.05, compared with control, Student's t test.

(C) Quantitative real-time PCR for synapse-related genes, *Homer1*, *Psd95*, and *Syn*, in THz-irradiated neurons and control cultures. Data are mean ± SEM of transcript levels relative to control after normalization from three independent experiments each performed in triplicate. **, p < 0.01, compared with control, Student's t test.

(D) Representative images of immunostaining of Tuj1 and Homer1 in 6-DIV low-density cultures after THz irradiation. Scale bar, 40 μm.

(E) Quantification of the percentage of Homer1$^+$ cells within Tuj1$^+$ neurons in control and THz-irradiated cultures. Data are mean ± SEM (n = 3 independent experiments). **, p < 0.01 compared with control, Student's t test.

(F) Representative images of immunostaining of Tuj1 and Homer1 in 6-DIV high-density cultures after THz irradiation. Scale bar, 40 μm.

(G) Quantification of the density of Homer1$^+$ spots within Tuj1$^+$ neurons in control and THz-irradiated cultures. Data are mean ± SEM (n = 3 independent experiments). *, p < 0.05 compared with control, Student's t test.

(H) Western blot assay for Syn showed increased expression in THz-irradiated neuron cultures. Histogram shows fold change measured by densitometry in the THz group relative to control after normalization to β-actin levels. Data are mean ± SEM (n = 3 independent experiments).

**, p < 0.01, ***, p < 0.001, Student's t test.

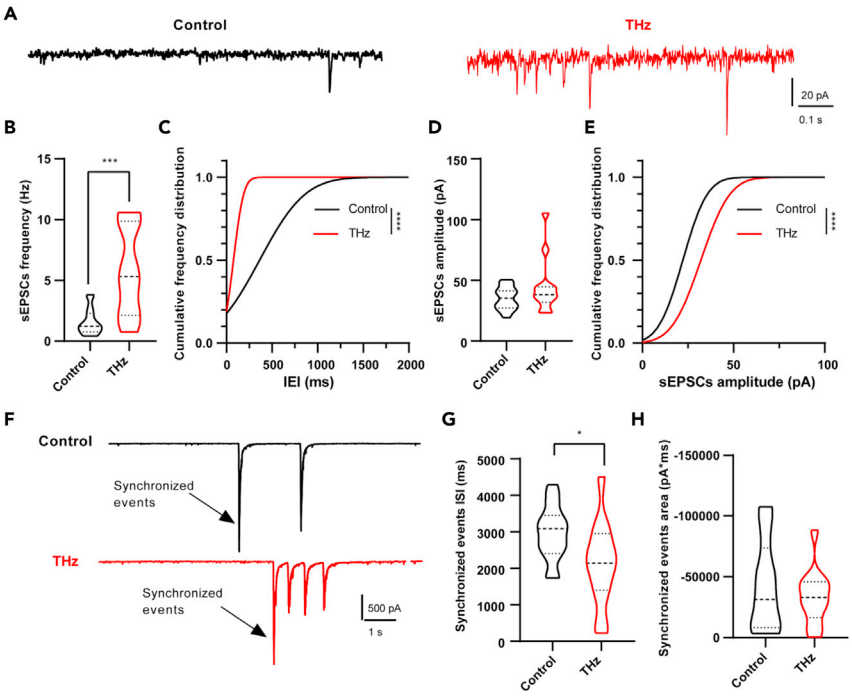

Figure 3. THz exposure promotes excitatory synaptic transmission

(A) Representative traces of sEPSCs recording in control and THz groups.

(B) The average frequency of sEPSCs from the THz group showed bigger value than that from the control group (Control: 1.6 ± 0.28 Hz, n = 15 cells; THz: 5.8 ± 1.06 Hz, n = 12 cells). Data are mean ± SEM, ***, $p < 0.001$, unpaired t test.

(C) The cumulative frequency distribution curve of sEPSCs frequency from the THz group shifted left compared with the curve of the control group. ****, $p < 0.0001$, Extra sum-of-squares F test.

(D) The average amplitude of sEPSCs from the THz group showed similar value with control group (Control: 35.3 ± 2.44 pA, n = 15 cells; THz: 45.1 ± 6.70 pA, n = 12 cells; unpaired t test, $p = 0.15$). Data are mean ± SEM.

(E) The cumulative frequency distribution curve of sEPSCs amplitude from the THz group shifted right compared with the curve of the control group. ****, $p < 0.0001$, Extra sum-of-squares F test.

(F) Representative traces of sEPSCs synchronized events in the control and THz groups.

(G) THz-irradiated neurons showed decreased inter-spike interval (ISI) of synchronized sEPSCs events compared with the control group (Control: 2,975 ± 192.1 ms, n = 15 cells; THz: 2,121 ± 340.1 ms, n = 12 cells). Data are mean ± SEM. *, $p < 0.05$, unpaired *t* test.

(H) The area of synchronized sEPSCs events did not show significant difference between the THz and control groups (Control: −43,522 ± 9,437 pA·ms, n = 15 cells; THz: −33,858 ± 6,729 pA·ms, n = 12 cells). Data are mean ± SEM.

See also Figure S3.

when the current injection reached the rheobase. And the AP amplitude of DFNs showed constant reduction during the repeat firing in the DFNs (Figure 4A). For the DFNs, the passive properties of the THz group and control group, including resting membrane potential (RMP), membrane resistance (Rm), and membrane capacitance (Cm), showed similar values (Figures 4B–4D). To test the active properties of these neurons, we did a current injection to keep the RMP of these neurons around −60 mV. We calculated the slope of the holding current and membrane voltage changes and found that the slope of the THz group was larger than in the control group (Figure 4E), which suggested that the holding efficiency of the THz group is higher than that of the control group. And we found that the rheobase of neurons from the THz group was lower than that from the control group (Figure 4F). The other parameters, including the threshold, the first spike delay time, the half width, and the peak of the action potential, all did not show a significant difference between the control and THz groups (Figures 4G–4J). Since the neurons of the THz group showed small rheobase, then we did the current injection-firing number curve to test whether the THz group could fire easier than the control group. Indeed, we found that the neurons in THz group generated more AP numbers compared with the control group at the same current injection intensity (Figures 4K and 4L). To further explore the potential neuronal mechanisms of firing property changes in DFNs, we compared the rising slope and decay slope of AP between the control and THz radiation groups. We did not find

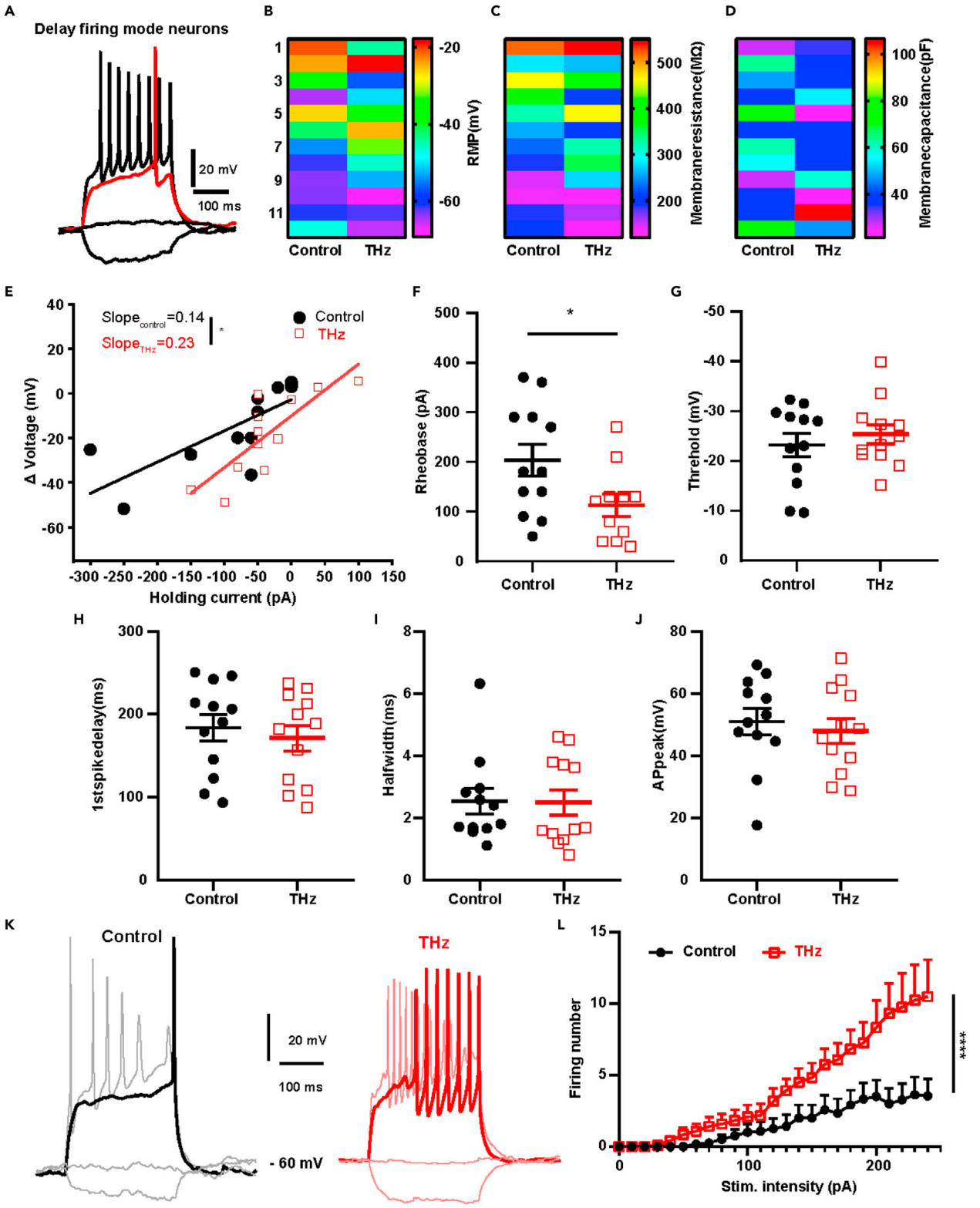
A
Delay firing mode neurons
20 mV
100 ms
B
RMP(mV)
Control
THz
C
Membraneresistance(MΩ)
Control
THz
D
Membranecapacitance(pF)
Control
THz
E
Slope control =0.14
Slope THz =0.23
Control
THz
Δ Voltage (mV)
Holding current (pA)
F
Rheobase (pA)
Control
THz
G
Threhold (mV)
Control
THz
H
1stspikedelay(ms)
Control
THz
I
Halfwidth(ms)
Control
THz
J
APpeak(mV)
Control
THz
K
Control
THz
20 mV
100 ms
- 60 mV
L
Control
THz
Firing number
Stim. intensity (pA)
****

Figure 4. THz exposure enhances firing properties of delay firing mode neurons (DFNs)

(A) Representative traces of current clamp recording from a DFN.

(B–D) THz-irradiated neurons showed similar value of the resting membrane potential (B), the membrane resistance (C), and the membrane capacitance (D) with the control group (RMP: control, −47.2 ± 4.86 mV, n = 12 cells; THz, −46.6 ± 4.68 mV, n = 12 cells. unpaired t test, p = 0.93; Rm: control, 276.1 ± 35.40 MΩ, n = 12; THz, 284.7 ± 38.99 mV, n = 12. unpaired t test, p = 0.87; Cm: control, 49.0 ± 5.09 pA, n = 12; THz, 44.5 ± 6.47 pA, n = 12. unpaired t test, p = 0.59). Data are mean ± SEM.

(E) THz-irradiated neurons showed bigger slope of delta voltage-holding current relationship compared with the control group ($Slope_{control}$ = 0.14, $Slope_{THz}$ = 0.23). Data are mean ± SEM. *, p < 0.05, F-test.

(F) THz-irradiated neurons showed smaller rheobase compared with the control group (Control: 203.3 ± 31.68 pA, n = 12 cells; THz: 112.7 ± 22.65 pA, n = 11 cells). Data are mean ± SEM. *, p < 0.05, Two-tailed unpaired t test.

(G–J) THz-irradiated neurons showed similar value of the AP threshold (G), the first spike delay time (H), AP half-width (I), and the AP peak (J) with the control group.

(K-L) THz-irradiated neurons generated more spikes compared with control neurons at the same stimulation of current injection. Data are mean ± SEM. ****, p < 0.0001, two-way ANOVA; p < 0.05 started at sti. Intensity >170 pA, post hoc Sidak's multiple comparisons test.

See also Figures S4 and S5.

any difference of the AP slopes between two groups in DFNs (Figures S5A and S5B). However, for the RFNs, the above-mentioned parameters did not show a significant difference between the control and THz groups (Figures S4, S5C, and S5D).

These results suggest that THz irradiation enhances neuronal activities of DFNs but leaves RFNs relatively insusceptible. And the effect may be not achieved by the intrinsic properties of the neuron itself but by excitatory synaptic transmission.

THz irradiation alters neuronal gene expression dynamics

To understand the molecular underpinnings of the observed morphology and electrophysiology changes in THz-irradiated neuron cultures, we compared the gene expression dynamics of control and THz-irradiated neurons. The irradiation plan identical to the electrophysiology study was used. There were 543 genes upregulated and 706 genes downregulated in THz-irradiated neurons compared with the control (p < 0.05, Log2 > 1 or < −1) (Figures 5A and 5B). As indicated by Gene Ontology (GO) analysis and Kyoto Encyclopedia of Genes and Genomes (KEGG) pathway analysis, among the top upregulated genes were those pertinent to neuron projection, synapse organization, and dendritic spine (Figure 5C). However, genes associated with actin binding, cytoskeleton organization, and response to stimulus were enriched in downregulated GO terms (Figure 5D). Quantitative PCR confirmed representative gene expression changes associated with these GO terms in the microarray data (Figure 5E). The gene expression dynamics of THz-irradiated neurons were in line with our observations on neuronal morphological and functional changes.

Long-term THz irradiation inhibits oligodendrocyte precursor cell proliferation

Along with neurons, there are other non-neuronal cells in the central nervous system (CNS) that support neuronal function. Oligodendrocytes (OLs) are the myelinating cells in the CNS and form myelin structures on the axons, which insulates axons and increases the propagation rate of electrical impulses along the nerves. During development, OLs arise after successive stages of lineage progression from oligodendrocyte precursor cells (OPCs) to immature OLs and finally to mature myelinating OLs (Nave and Werner, 2014). OPCs are mitotic cells and we first test the effect of THz exposure on OPC proliferation, by BrdU incorporation assay.

Similar to the THz irradiation plan for neuron cultures, we applied both short- (15 min × 3 times a day) and long- (3 h one time a day) term exposure on OPCs. Cells were maintained in proliferating medium, irradiated for 2 days (1 and 2 DIV), and subjected to analysis at 3 DIV (Figure 6A). Four hours before culture fixation, BrdU was added into the medium to label the proliferating cells. Under short-term irradiation conditions, we did not observe a significant difference in the percentage of $BrdU^+$ cells among $Olig2^+$ cells, which is an oligodendrocyte lineage marker, between the control and THz group (Figures 6B and 6C). However, long-term exposure significantly decreased the percentage of $BrdU^+$ cells among $Olig2^+$ cells (Figures 6D–6F). These results indicate that THz irradiation may inhibit OPC proliferation under certain conditions.

THz exposure enhances oligodendrocyte differentiation and myelination

To further test if THz irradiation has an impact on the differentiation process of OLs, we examined the expression of OL marker at the different stages after THz exposure. OLs were maintained in differentiation

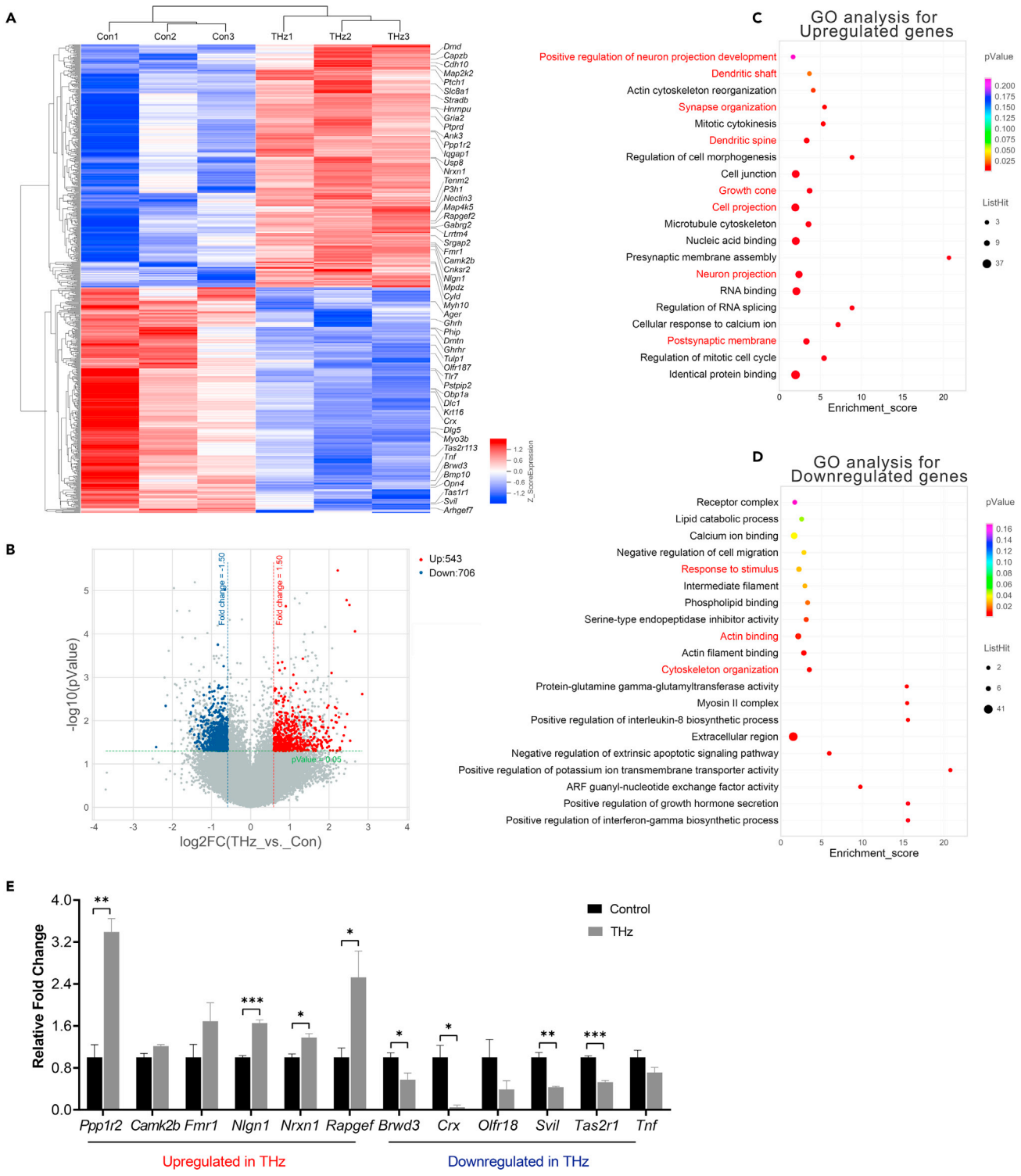

Figure 5. THz irradiation alters gene expression dynamics in neurons

(A) Heatmap of microarray data from neurons show categories of differentially expressed genes between control and THz groups. Each treatment was repeated three times.

(B) Volcanic plot of the differentially expressed genes in THz-irradiated neurons and control neurons.

(C) Gene ontology analysis of top 20 upregulated gene groups in THz-irradiated neuron cultures.

(D) Gene ontology analysis of top 20 downregulated gene groups in THz-irradiated neuron cultures.

Figure 5. *Continued*

(E) Quantitative real-time PCR for representative genes revealed by microarray in THz-irradiated neurons and control cultures. Data are mean ± SEM of transcript levels relative to control after normalization from three independent experiments each performed in triplicate. *, $p < 0.05$, **, $p < 0.01$, ***, $p < 0.001$, compared with control, Student's t test.

medium after plating and daily THz exposure was started from 2 DIV. For short-term irradiation, cultures were fixed at 3, 4, and 5 DIV for immunostaining OPC marker, PDGFRα, immature OL marker, CNPase, and mature OL marker, myelin basic protein (MBP) (Figure S6A). Similar to the proliferation results, we did not reveal significant changes in the density of $CNPase^+$ and MBP^+ cells at time points (Figures S6B–S6D). However, we did show a significant increase in the percentage of $CNPase^+$ and MBP^+ cells at 5 DIV in the long-term irradiation group (Figures 7A–7C). Quantitative real-time PCR confirmed the upregulation of *Cnp* and *Mbp* expression at the mRNA level in the THz group (Figure 7D). Together with the above-mentioned OPC proliferation results, we speculate that long-term THz exposure can inhibit OPCs proliferation and enhance their differentiation.

In addition, we tested the ability of oligodendrocyte to form myelin on neuronal cultures after THz irradiation. Neuron cultures were irradiated with THz from 2 to 4 DIV under long-term irradiation protocol and purified OPCs were added into neurons at 5 DIV; the co-cultures were irradiated for two more days and subjected to immunostaining at 14 DIV (Figure 7E). We noticed that, in the control cultures at 14 DIV, only few OLs formed long myelin alone axons, most OLs synthesized short myelin around the cell body at this time point (Figure 7F). However, THz irradiation significantly promoted myelination and long myelins were prominent in the co-cultures (Figures 7F and 7G). These observations suggest that THz irradiation enhances the cross talk between neurons and oligodendrocytes, then accelerates the process of myelination.

DISCUSSION

A number of studies have explored THz radiation effects on biological functions and several reviews have summarized these studies (Zhao et al., 2014a; Wilmink and Grundt, 2011). It is clear from these reviews that cell types, exposure characteristics (frequency, power, duration, etc.), and thermal conditions vary greatly between these studies, which makes it difficult to draw general conclusions. In the current study, in order to ensure THz exposures are conducted in an accurate, controlled, and reproducible fashion, we applied a temperature-controlled exposure chamber to achieve high-quality *in vitro* THz biological studies. The exposure chamber serves several important purposes. First, it ensures that the biological samples are maintained under appropriate homeostatic conditions (37°C, 95% humidity, and 5% CO_2) during THz exposures. Maintenance of homeostatic conditions is of paramount importance because mammalian cells undergo stress responses when exposed to room temperature conditions (Watanabe and Okada, 1967; Neutelings et al., 2013). As a result, such conditions can lead to biological effects that may be artifacts. Thus, when exposure chambers are omitted, it becomes difficult to determine whether the observed biological effects are a direct result of the THz radiation or are due to the non-homeostatic environmental conditions. In addition, exposure chambers can also provide constant CO_2 levels, which is important for keeping extracellular pH levels.

In the current study, we did not observe a cytotoxic effect of THz exposure on both mouse primary cortical neurons and oligodendrocytes with a power density of 70 $\mu W/cm^2$, revealed by TUNEL staining. Some reports suggested that power intensity at the mW/cm^2 level may produce the cytotoxic effect. For example, a dose-dependent cytotoxic effect of continuous THz radiation (0.12–0.18 THz, average power density of 3.2 mW/cm^2) was demonstrated on a rat glial cell line (Borovkova et al., 2017); the cell death of isolated neurons from the *Lymnea stagnalis* occurred 3 h after exposure to 2.3-THz waves at 3 mW/cm^2 intensity (Cherkasova et al., 2021), whereas the low power intensity, around $\mu W/cm^2$ level, was considered relatively safer to the cells *in vitro*. For example, exposure to the mean intensity of 8–200 $\mu W/cm^2$ within the frequency range of 0.1–6.5 THz will not cause DNA damage in human blood leukocytes (Angeluts et al., 2014); the sensory ganglion of chicken embryos showed obvious nerve fiber growth under 0.05–2 THz radiation with 0.5 $\mu W/cm^2$ intensity (Tsurkan et al., 2012). However, experiments with different biological targets also showed contradicting results after exposing to THz radiation of similar frequency (0.10–0.15 THz) and power density (0.04–5 mW/cm^2) (Borovkova et al., 2017; Koyama et al., 2016; De Amicis et al., 2015; Clothier and Bourne, 2003; Olshevskaya et al., 2009), indicating that the properties and characteristics of biological samples may also determine the cytotoxic effects. From previous findings and our results, we believe that current parameters of THz irradiation are safe to study the biological effects of neurons and oligodendrocytes *in vitro*.

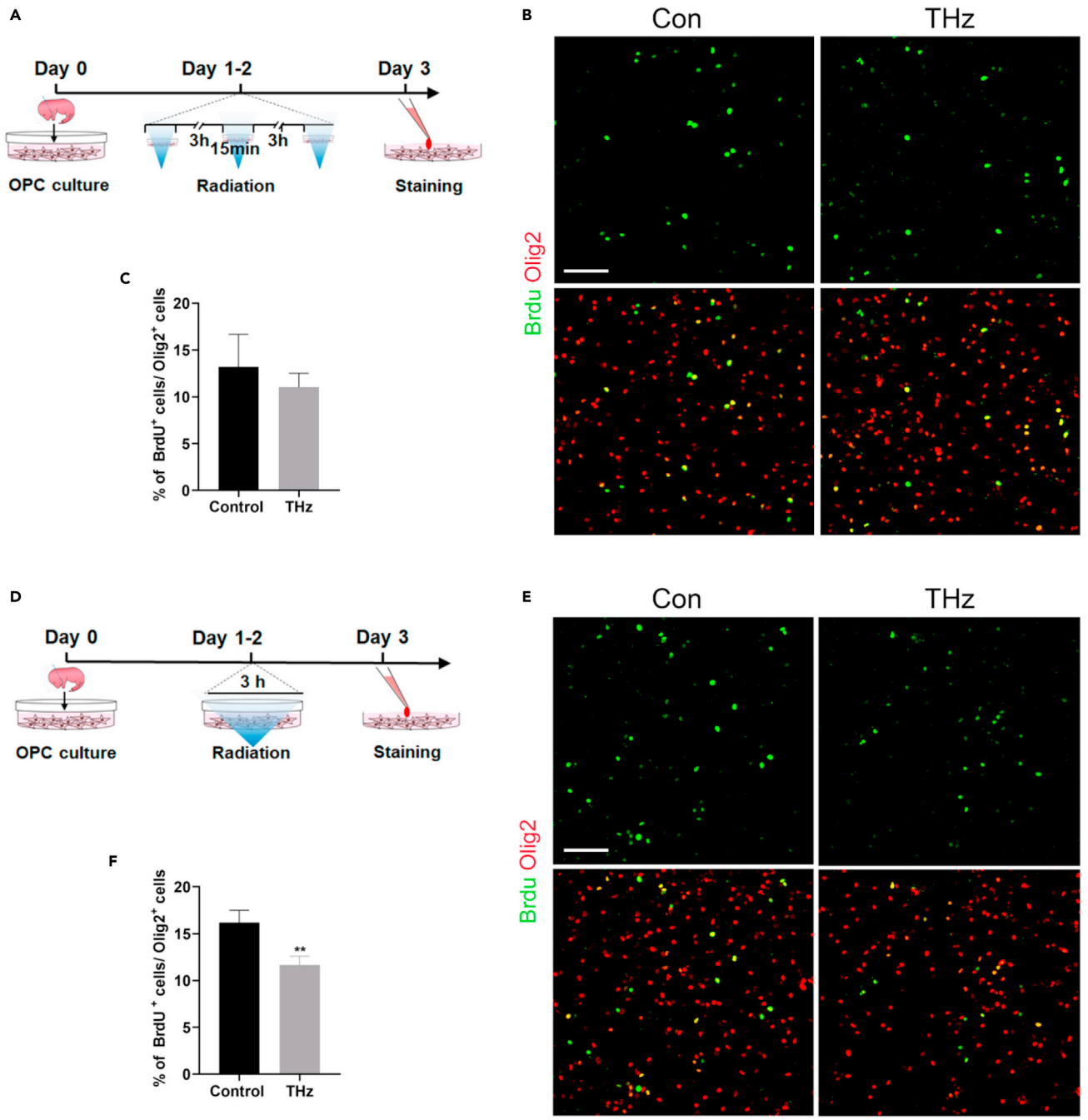

Figure 6. Long-term THz irradiation inhibits OPC proliferation

(A) Diagram showing short-term THz irradiation on OPCs for immunostaining assay.

(B) Representative images of immunostaining for BrdU and Olig2 in 3-DIV OPCs after short-term THz irradiation. Scale bar, 50 μm.

(C) Percentage of $BrdU^+$ cells among $Olig2^+$ cells in cultures from control or THz-irradiated groups. Data are mean ± SEM ($n = 3$ of independent experiments each group). *n.s*, Student's t test.

(D) Diagram showing long-term THz irradiation on OPCs for immunostaining assay.

(E) Representative images of immunostaining for BrdU and Olig2 in 3-DIV OPCs after long-term THz irradiation. Scale bar, 50 μm.

(F) Percentage of $BrdU^+$ cells among $Olig2^+$ cells in cultures from control or THz-irradiated groups. Data are mean ± SEM ($n = 3$ of independent experiments each group).

**, $p < 0.01$, Student's t test.

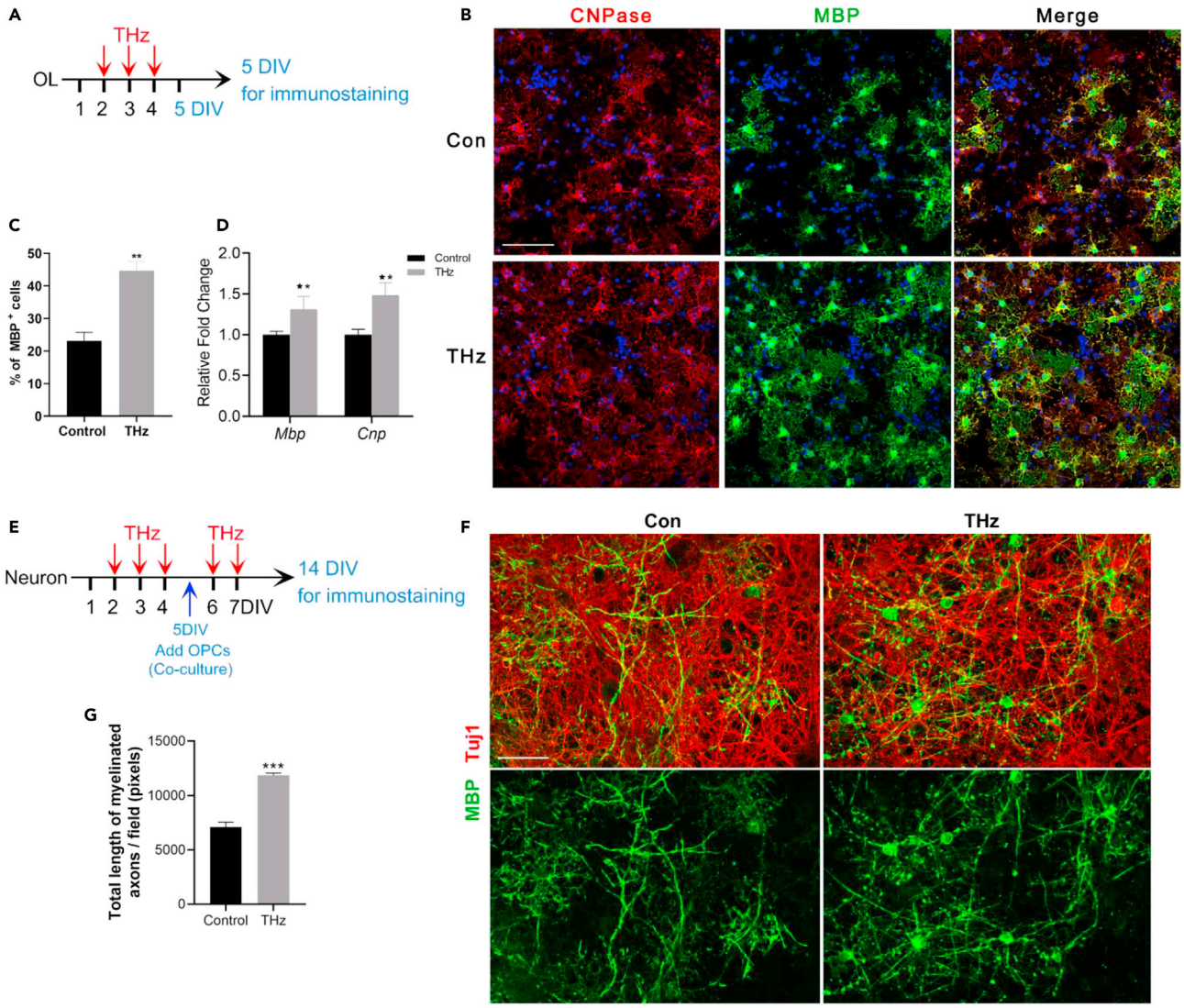

Figure 7. Long-term THz irradiation enhances OL differentiation and myelination

(A) Diagram showing long-term THz irradiation and succeeding analysis for OL.

(B) Representative images of immunostaining for CNPase and MBP at 5 DIV after THz irradiation. Scale bar, 50 μm.

(C) Percentage of $CNPase^+$ and MBP^+ cells in OL cultures from control and THz-irradiated groups. Data are mean ± SEM ($n = 3$ of independent experiments each group). **, $p < 0.01$, Student's t test.

(D) Quantitative real-time PCR of *Mbp* and *Cnp*, in THz-irradiated OLs and control cultures. Data are mean ± SEM of transcript levels relative to control after normalization from three independent experiments each performed in triplicate. **, $p < 0.01$, compared with control, Student's t test.

(E) Diagram showing long-term THz irradiation on neuron-OL co-cultures for immunostaining.

(F) Representative images of immunostaining for Tuj1 and MBP at 14 DIV co-cultures after THz irradiation. Scale bar, 50 μm.

(G) Quantification of the length of myelin in defined area between the control and THz groups. Data are mean ± SEM (n = 3 independent experiments). ***, $p < 0.001$, compared with control, Student's t test.

See also Figure S6.

As to the functional effects of THz irradiation, our observations demonstrate that neuron cultures exhibit a significantly increased expression of synaptic-associated proteins, e.g., Homer1 and Synapsin, with either short- or long-term irradiation. Meanwhile, microarray assay revealed that genes associated with "neuron projection," "synapse organization," and "dendritic spine" were upregulated in THz-irradiated neurons. There are several studies that tested THz effects on primary neuronal cultures. For example, a research examining isolated neurons from *Lymnaea stagnalis* has revealed that multiple functions, including cellular growth, adhesion, membrane morphology, intracellular structures, excitatory synaptic

transmission, and neuronal firing activities, were affected by THz radiation in a dose-dependent manner (Olshevskaya et al., 2009). In this study, exposures were conducted with a THz FEL using the following parameters: frequencies of 0.7, 2.49, and 3.69 THz; H = 0.3–30 mW/cm^2, exposure time ≥1 min. Another study compared the potential effects of THz on primary rat neuron cultures from different brain regions and on three kinds of neuron-like cell lines (Tan et al., 2019). With an output power of 50 mW (0.16 THz) and 10 mW (0.17 THz), short-term (6 and 60 min) exposure induced significant neurotransmitter changes, e.g., Glu, Ala, and Gly, in hippocampal, cerebellar, brainstem neurons and in MN9D and PC12 cells. A recent study investigating the gene expression changes after THz radiation in primary rat hippocampus neurons revealed that biomolecule binding-related gene categories such as "long-chain fatty acid binding," "tropomyosin binding," "BMP receptor binding," "GTPase binding," and "phospholipid binding" were enriched by GO analysis (Shang et al., 2021). These studies present different aspects of THz radiation effects on neurons under different exposure power, from molecular to morphology response, thus indicating the significance of exploring the broad effects and underlying mechanism of THz irradiation in detail.

Consistent with the morphology and transcriptome changes, we found that THz irradiation enhanced the excitatory synaptic transmissions and synchronization. Increased excitatory synaptic activities could promote neuronal activities. We observed increased firing in the DFNs, caused by the reduced rheobase after THz exposure. But we did not find either rise slope or decay slope of AP changes in the DFNs. This suggested that the enhanced neuronal activities of DFNs may be caused by increased excitatory synaptic transmission, but not the neuronal intrinsic properties, since we did not block the synaptic activities during the evoked AP recording. And both the synaptic proteins and excitatory synaptic function also significantly increased in THz group. However, the RFNs showed similar firing properties with the control group. We did not know the exact reason that THz exposure showed differential effects on these two firing mode types of neurons. One possibility is that different type neurons may show different sensitivity to THz irradiation. Actually, we noticed that RFNs in the THz group tend to generate more APs at higher current stimulation intensity (Figure S4L), although the statistics did not reach to significant difference. Interestingly, a recent work reported that midinfrared 53.6 THz (wavelength 5.6 μm) radiation with ∼110 μW/μm^2 density increases neuronal firing through voltage-gated potassium channel, by acting on resonance vibration of –C = O bonds at the potassium channel (Liu et al., 2021). And this result is a non-thermal effect of midinfrared wave. The difference between the current work and their observations may come from several factors, such as wavelength, power density, and the radiation protocol. Further work needs to be done by exploring the effect on the neuronal activities and synaptic transmission with different radiation paradigm even in the 3.1-THz laser.

As to oligodendrocytes, we tested both short- and long-term irradiation protocol but only detected significant changes in OPC proliferation and differentiation after long-term THz irradiation. The different response to short-term irradiation between neurons and oligodendrocyte thus indicates a cell-type-specific effect under certain conditions, e.g., neurons are excitable cells and could be more easily stimulated by short-term THz exposure than OLs. THz effects on cell proliferation and differentiation have been another debating issue. It was found that THz radiation (frequencies up to ∼0.5 THz with peak powers up to 11.5 kW and average powers up to 1.2 mW) had no significant effect on proliferation and differentiation of certain cells *in vitro*, like epithelial and embryonic stem cell lines (Williams et al., 2013). However, study using a similar cell type, mouse stem cells, showed that a broad-spectrum THz radiation (centered at ∼10 THz with an average power density of ∼1 mW/cm^2) for 2 and 6 h accelerates stem cell differentiation toward adipose phenotype (Bock et al., 2010). We also noticed that a single-cycle THz pulses (5 μJ energy, 0.30 THz mean frequency, 293 kV/cm peak electric field, and 1 kHz repetition rate) stimulated the cell proliferation in an earthworm regeneration model (Abufadda et al., 2021). Together with our results, it is hard to draw conclusions about THz effects on cell proliferation and differentiation at the current stage, and we believe that THz radiation may have a strong and versatile influence on biological system, depending on the irradiation parameters and on the characteristics of the biological targets as suggested in previous studies (Abufadda et al., 2021).

Besides, the long-term THz irradiation protocol for neuron-OL co-cultures prominently enhanced myelin formation. This observation is highly consistent with previous studies that inducing neuronal activity via electrical stimulation can promote axon myelination (Malone et al., 2013; Stevens et al., 2002; Zalc and Fields, 2000) and in line with the results that THz irradiation can promote neuronal activity in our study.

Also, the enhanced myelination can be explained by increased myelin protein expression in purified OL cultures after THz exposure. Interestingly, a recent study provides the model for explaining the mechanism of infrared and terahertz neurotransmission through myelinated nerves (Liu et al., 2019), which may help our understanding of neural information transduction in the central nervous system.

Although the underlying mechanism for THz waves on neurons and OLs remains unclear, we have excluded the possible temperature increase during THz exposure. With a fast response and laboratory accuracy thermometer (0.05% + 0.3°C), we did not reveal significant temperature rise during 3-h exposure to THz radiation. Besides, the most common thermal effects observed at a cellular level include the stimulation of cell growth and metabolism, morphological changes, activation of cellular stress response mechanism (CSR), and cell death via apoptotic and necrotic pathways (Wilmink and Grundt, 2011). CSR mechanisms involve many intracellular pathways, and a group of 44 evolutionarily conserved proteins has emerged as core mediators (Kultz, 2005). These proteins, collectively referred to as minimal stress proteins, are significantly upregulated by cells immediately after exposure to stress. The most widely studied family of minimal stress proteins are the heat shock proteins (Hsps), including Hsp70, Hsp40, Hsp60, and Hsp105 (Beckham et al., 2010). None of these genes were detected in our microarray data as well as RT-PCR assay, indicating the minimal thermal effects on neurons and OLs.

In conclusion, we found that 3.1 THz irradiation could enhance the neurite outgrowth and synaptic-associated genes and increase excitatory synaptic transmissions under both short- and long-term exposure duration. And the spike activities of a certain type of neuron also showed increased firing activities. In line with these findings, the gene expression of THz-irradiated neurons also demonstrated dynamic changes including actin binding, cytoskeleton organization, and response to stimulus pathways. However, long-term THz exposure produced a different effect on OPCs. It inhibits OPCs proliferation and enhances their differentiation. Our results suggested that THz irradiation could induce a complicated biological effect on the nervous system, which still needs further investigation.

Limitations of the study

Although we have observed the neuronal transcriptome changes after 3.1-THz exposure, the detailed mechanisms for the regulation of gene expression are not clear. A set of studies have suggested that numerous biomolecules interactions might be affected by THz radiation, especially, the interactions among transcription factors that play a vital role in activating the transcription initiation might be the targets of THz radiation (Homenko et al., 2009). Besides, the DNA breathing model provides one of the many possible underlying mechanisms: THz radiation may create new open states in the DNA helix through nonlinear resonance and therefore influence gene expression (Alexandrov et al., 2010, 2013). A recent study indicated that terahertz stimulus at a characteristic frequency (44.0 THz) can be used as an efficient method to accelerate the unwinding process of DNA duplexes (Wu et al., 2020). The mechanism was revealed to be the resonance between the terahertz stimulus and the vibration of purine connected by the weak hydrogen bond and the consequent break in hydrogen bond connections between these base pairs. Besides, the THz wave has been suggested to enhance permeability of the voltage-gated calcium channel by resonance effect (Li et al., 2021), which may increase Ca^{2+} permeation and induce the gene transcription. Thus, these observations may provide possible explanation for our current results about transcriptome dynamics after THz exposure in neuronal cultures.

More molecular assays, such as ChIP-seq analysis, are required to explore the transcriptional or epigenetic regulation on gene expression after THz exposure, which is far beyond our current study and is restricted by the relatively limited irradiation spot area. We will try to test in further study with a novel THz source that can provide a wider irradiation range and enough cell numbers required for molecular assays.

STAR★METHODS

Detailed methods are provided in the online version of this paper and include the following:

- KEY RESOURCES TABLE
- RESOURCE AVAILABILITY
  - Lead contact
  - Materials availability
  - Data and code availability

SUPPLEMENTAL INFORMATION

Supplemental information can be found online at https://doi.org/10.1016/j.isci.2021.103485.

ACKNOWLEDGMENTS

The authors would like to thank Dr. Fangfang Liu, Dr. Lirong Liang, and Dr. Jinshuan Zhang for their great technical support. This work was funded by grants from the National Natural Science Foundation of China (Grant number: 82071271 and 31571050 to X.Z., 81730035 to S.W., 81771476 and 82071536 to W.W.).

AUTHOR CONTRIBUTIONS

W.W., H.Z., X.Z., and S.W. contributed to experimental design and discussion. W.W., M.Z., Y.L., K.R., and Q.X. performed the experiments and collected data. W.W., M.Z., H.L., and X.Z. analyzed data. W.W., X.Z., and S.W. wrote, edited, and reviewed the manuscript. All authors read and approved the final manuscript.

DECLARATION OF INTERESTS

The authors declare that there are no conflicts of interests.

Received: June 25, 2021
Revised: October 6, 2021
Accepted: November 19, 2021
Published: December 17, 2021

REFERENCES

Abufadda, M.H., Erdelyi, A., Pollak, E., Nugraha, P.S., Hebling, J., Fulop, J.A., and Molnar, L. (2021). Terahertz pulses induce segment renewal via cell proliferation and differentiation overriding the endogenous regeneration program of the earthworm *Eisenia andrei*. Biomed. Opt. Express *12*, 1947–1961. https://doi.org/10.1364/BOE.416158.

Alexandrov, B.S., Gelev, V., Bishop, A.R., Usheva, A., and Rasmussen, K.O. (2010). DNA breathing dynamics in the presence of a terahertz field. Phys. Lett. A *374*, 1214. https://doi.org/10.1016/j.physleta.2009.12.077.

Alexandrov, B.S., Phipps, M.L., Alexandrov, L.B., Booshehri, L.G., Erat, A., Zabolotny, J., Mielke, C.H., Chen, H.T., Rodriguez, G., Rasmussen, K.O., et al. (2013). Specificity and heterogeneity of terahertz radiation effect on gene expression in mouse mesenchymal stem cells. Sci. Rep. *3*, 1184. https://doi.org/10.1038/srep01184.

Angeluts, A.A., Gapeyev, A.B., Esaulkov, M.N., Kosareva, O.G., Matyunin, S.N., Nazarov, M.M., Pashovkin, T.N., Solyankin, P.M., Cherkasova, O.P., and Shkurinov, A.P. (2014). Study of terahertz-radiation-induced DNA damage in human blood leukocytes. Quan. Elec. (Woodbury) *44*, 247–251. https://doi.org/10.1070/QE2014v044n03ABEH015337.

Beckham, J.T., Wilmink, G.J., Opalenik, S.R., Mackanos, M.A., Abraham, A.A., Takahashi, K., Contag, C.H., Takahashi, T., and Jansen, E.D. (2010). Microarray analysis of cellular thermotolerance. Lasers Surg. Med. *42*, 752–765. https://doi.org/10.1002/lsm.20983.

Bock, J., Fukuyo, Y., Kang, S., Phipps, M.L., Alexandrov, L.B., Rasmussen, K.O., Bishop, A.R., Rosen, E.D., Martinez, J.S., Chen, H.T., et al. (2010). Mammalian stem cells reprogramming in response to terahertz radiation. PLoS One *5*, e15806. https://doi.org/10.1371/journal.pone.0015806.

Bondar, N.P., Kovalenko, I.L., Avgustinovich, D.F., Khamoyan, A.G., and Kudryavtseva, N.N. (2008). Behavioral effect of terahertz waves in male mice. Bull. Exp. Biol. Med. *145*, 401–405. https://doi.org/10.1007/s10517-008-0102-x.

Borovkova, M., Serebriakova, M., Fedorov, V., Sedykh, E., Vaks, V., Lichutin, A., Salnikova, A., and Khodzitsky, M. (2017). Investigation of terahertz radiation influence on rat glial cells. Biomed. Opt. Express *8*, 273–280. https://doi.org/10.1364/boe.8.000273.

Bourne, N., Clothier, R.H., D'arienzo, M., and Harrison, P. (2008). The effects of terahertz radiation on human keratinocyte primary cultures and neural cell cultures. Altern. Lab. Anim. *36*, 667–684. https://doi.org/10.1177/026119290803600610.

Cherkasova, O.P., Serdyukov, D.S., Nemova, E.F., Ratushnyak, A.S., Kucheryavenko, A.S., Dolganova, I.N., Xu, G., Skorobogatiy, M., Reshetov, I.V., Timashev, P.S., et al. (2021). Cellular effects of terahertz waves. J. Biomed. Opt. *26*. https://doi.org/10.1117/1.Jbo.26.9.090902.

Clothier, R.H., and Bourne, N. (2003). Effects of THz exposure on human primary keratinocyte differentiation and viability. J. Biol. Phys. *29*, 179–185. https://doi.org/10.1023/A:1024492725782.

De Amicis, A., Sanctis, S.D., Cristofaro, S.D., Franchini, V., Lista, F., Regalbuto, E., Giovenale, E., Gallerano, G.P., Nenzi, P., Bei, R., et al. (2015). Biological effects of in vitro THz radiation exposure in human foetal fibroblasts. Mutat. Res. Genet. Toxicol. Environ. Mutagen *793*, 150–160. https://doi.org/10.1016/j.mrgentox.2015.06.003.

Gardner, A., Jukkola, P., and Gu, C. (2012). Myelination of rodent hippocampal neurons in culture. Nat. Protoc. *7*, 1774–1782. https://doi.org/10.1038/nprot.2012.100.

Homenko, A., Kapilevich, B., Kornstein, R., and Firer, M.A. (2009). Effects of 100 GHz radiation on alkaline phosphatase activity and antigen-antibody interaction. Bioelectromagnetics *30*, 167–175. https://doi.org/10.1002/bem.20466.

Kirichuk, V.F., Efimova, N.V., and Andronov, E.V. (2009). Effect of high power terahertz irradiation on platelet aggregation and behavioral reactions of albino rats. Bull. Exp. Biol. Med. *148*, 746–749. https://doi.org/10.1007/s10517-010-0807-5.

Koyama, S., Narita, E., Shimizu, Y., Shiina, T., Taki, M., Shinohara, N., and Miyakoshi, J. (2016). Twenty four-hour exposure to a 0.12 THz electromagnetic field does not affect the genotoxicity, morphological changes, or expression of heat shock protein in HCE-T cells. Int. J. Environ. Res. Public Health *13*. https://doi.org/10.3390/ijerph13080793.

Kultz, D. (2005). Molecular and evolutionary basis of the cellular stress response. Annu. Rev. Physiol. *67*, 225–257. https://doi.org/10.1146/annurev.physiol.67.040403.103635.

Lesuisse, C., and Martin, L.J. (2002). Long-term culture of mouse cortical neurons as a model for neuronal development, aging, and death. J. Neurobiol. *51*, 9–23. https://doi.org/10.1002/neu.10037.

Li, Y., Chang, C., Zhu, Z., Sun, L., and Fan, C. (2021). Terahertz wave enhances permeability of the voltage-gated calcium channel. J. Am. Chem. Soc. *143*, 4311–4318. https://doi.org/10.1021/jacs.0c09401.

Liu, G.Z., Chang, C., Qiao, Z., Wu, K.J., Zhu, Z., Cui, G.Q., Peng, W.Y., Tang, Y.Z., Li, J., and Fan, C.H. (2019). Myelin sheath as a dielectric waveguide for signal propagation in the mid-infrared to terahertz spectral range. Adv. Funct. Mater. *29*. https://doi.org/10.1002/adfm.201807862.

Liu, X., Qiao, Z., Chai, Y., Zhu, Z., Wu, K., Ji, W., Li, D., Xiao, Y., Mao, L., Chang, C., et al. (2021). Nonthermal and reversible control of neuronal signaling and behavior by midinfrared stimulation. Proc. Natl. Acad. Sci. U S A *118*. https://doi.org/10.1073/pnas.2015685118.

Malone, M., Gary, D., Yang, I.H., Miglioretti, A., Houdayer, T., Thakor, N., and Mcdonald, J. (2013). Neuronal activity promotes myelination via a cAMP pathway. Glia *61*, 843–854. https://doi.org/10.1002/glia.22476.

Mazuir, E., Dubessy, A.L., Wallon, L., Aigrot, M.S., Lubetzki, C., and Sol-Foulon, N. (2020). Generation of oligodendrocytes and oligodendrocyte-conditioned medium for co-culture experiments. J. Vis. Exp. https://doi.org/10.3791/60912.

Nave, K.A., and Werner, H.B. (2014). Myelination of the nervous system: mechanisms and functions. Annu. Rev. Cell. Dev. Biol. *30*, 503–533. https://doi.org/10.1146/annurev-cellbio-100913-013101.

Neutelings, T., Lambert, C.A., Nusgens, B.V., and Colige, A.C. (2013). Effects of mild cold shock (25 degrees C) followed by warming up at 37 degrees C on the cellular stress response. PLoS One *8*, e69687. https://doi.org/10.1371/journal.pone.0069687.

Olshevskaya, J., Kozlov, A., Petrov, A., Zapara, T.A., and Ratushnyak, A. (2009). Influence of terahertz (submillimeter) laser radiation on neurons in vitro. Zh Vyssh Nerv Deiat Im I P Pavlova *59*, 342–348.

Romanenko, S., Begley, R., Harvey, A.R., Hool, L., and Wallace, V.P. (2017). The interaction between electromagnetic fields at megahertz, gigahertz and terahertz frequencies with cells, tissues and organisms: risks and potential. J. R. Soc. Interf. *14*. https://doi.org/10.1098/rsif.2017.0585.

Shang, S., Wu, X., Zhang, Q., Zhao, J., Hu, E., Wang, L., and Lu, X. (2021). 0.1 THz exposure affects primary hippocampus neuron gene expression via alternating transcription factor binding. Biomed. Opt. Express *12*, 3729–3742. https://doi.org/10.1364/boe.426928.

Smye, S.W., Chamberlain, J.M., Fitzgerald, A.J., and Berry, E. (2001). The interaction between terahertz radiation and biological tissue. Phys. Med. Biol. *46*, R101–R112. https://doi.org/10.1088/0031-9155/46/9/201.

Stevens, B., Porta, S., Haak, L.L., Gallo, V., and Fields, R.D. (2002). Adenosine: a neuron-glial transmitter promoting myelination in the CNS in response to action potentials. Neuron *36*, 855–868. https://doi.org/10.1016/s0896-6273(02)01067-x.

Tan, S.Z., Tan, P.C., Luo, L.Q., Chi, Y.L., Yang, Z.L., Zhao, X.L., Zhao, L., Dong, J., Zhang, J., Yao, B.W., et al. (2019). Exposure effects of terahertz waves on primary neurons and neuron-like cells under nonthermal conditions. Biomed. Environ. Sci. *32*, 739–754. https://doi.org/10.3967/bes2019.094.

Tsurkan, M., Smolyanskaya, O., Bespalov, V., Penniyainen, V., Kipenko, A., Lopatina, E., and Krylov, B. (2012). Changing growth of neurites of sensory ganglion by terahertz radiation. Proc. SPIE, 8261. https://doi.org/10.1117/12.909350.

Watanabe, I., and Okada, S. (1967). Effects of temperature on growth rate of cultured mammalian cells (L5178Y). J. Cell Biol. *32*, 309–323. https://doi.org/10.1083/jcb.32.2.309.

Williams, R., Schofield, A., Holder, G., Downes, J., Edgar, D., Harrison, P., Siggel-King, M., Surman, M., Dunning, D., Hill, S., et al. (2013). The influence of high intensity terahertz radiation on mammalian cell adhesion, proliferation and differentiation. Phys. Med. Biol. *58*, 373–391. https://doi.org/10.1088/0031-9155/58/2/373.

Wilmink, G.J., and Grundt, J.E. (2011). Invited review article: current state of research on biological effects of terahertz radiation. J. Infrared Millim. Terahertz Waves *32*, 1074–1122. https://doi.org/10.1007/s10762-011-9794-5.

Wu, K.J., Qi, C.H., Zhu, Z., Wang, C.L., Song, B., and Chang, C. (2020). Terahertz wave accelerates DNA unwinding: a molecular dynamics simulation study. J. Phys. Chem. Lett. *11*, 7002–7008. https://doi.org/10.1021/acs.jpclett.0c01850.

Zalc, B., and Fields, R.D. (2000). Do action potentials regulate myelination? Neuroscientist *6*, 5–13. https://doi.org/10.1177/107385840000600109.

Zhao, F.Y., Li, Y.Y., Liu, J.Q., Liu, F.Q., Zhang, J.C., Zhai, S.Q., Zhuo, N., Wang, L.J., Liu, S.M., and Wang, Z.G. (2019). Sampled grating terahertz quantum cascade lasers. Appl. Phys. Lett. *114*. https://doi.org/10.1063/1.5066310.

Zhao, L., Hao, Y.H., and Peng, R.Y. (2014a). Advances in the biological effects of terahertz wave radiation. Mil. Med. Res. *1*, 26. https://doi.org/10.1186/s40779-014-0026-x.

Zhao, X., Dai, J., Ma, Y., Mi, Y., Cui, D., Ju, G., Macklin, W.B., and Jin, W. (2014b). Dynamics of ten-eleven translocation hydroxylase family proteins and 5-hydroxymethylcytosine in oligodendrocyte differentiation. Glia *62*, 914–926. https://doi.org/10.1002/glia.22649.

STAR★METHODS

KEY RESOURCES TABLE

REAGENT or RESOURCE	SOURCE	IDENTIFIER
Antibodies		
Mouse anti-Tuj1	R&D systems	Cat# MAB1195 RRID: AB_2256751
Mouse anti-CNPase	Biolegend	Cat# 836404 RRID: AB_476854
Rat anti-MBP	Abcam	Cat# ab7349 RRID: AB_305869
Mouse anti–β-actin	Sigma	Cat# A2228 RRID: AB_476697
Rabbit anti-Homer1	Abcam	Cat# ab184955 RRID: AB_2744679
Rabbit anti-PDGFRα	BD Pharmingen	Cat# 558774 RRID: AB_2162341
Rabbit anti-Olig2	Millipore	Cat# AB9610 RRID: AB_570666
Rabbit anti-Synaptophysin	Abcam	Cat# ab32127 RRID: AB_2286949
Anti BrdUrd	DSHB	Cat# G3G4 RRID: AB_2618097
HRP, Goat Anti-Rabbit IgG	Abbkine	Cat# A21020
HRP, Goat Anti-Mouse IgG	Abbkine	Cat# A21010
Chemicals, peptides, and recombinant proteins		
poly-D-lysine	Sigma	Cat# P7405
poly-l-ornithine	Sigma	Cat# P0421
Neurobasal™ Plus Medium	Thermo Fisher	Cat# A3582901
B27 plus	Thermo Fisher	Cat# A3582801
N2-supplement	Thermo Fisher	Cat# 17502048
Glutamine	Sigma	Cat# G8540
Penicillin-Streptomycin	Thermo Fisher	Cat# 15140122
DMEM-high glucose medium	Thermo Fisher	Cat# 11995065
DMEM/F12	Thermo Fisher	Cat# 11330032
Fetal bovine serum	Thermo Fisher	Cat# HS300700
GlutaMAX	Thermo Fisher	Cat# 35050061
Sodium pyruvate	Sigma	Cat# P2256
Bovine serum albumin	Sigma	Cat# A9647
Insulin	Sigma	Cat# I6634
Biotin	Sigma	Cat# B4501
Apo-Transferrin	Sigma	Cat# T2252
Sodium selenate	Sigma	Cat# S5261
N-acetyl-L-cysteine (NAc)	Sigma	Cat# A-8199
Ciliary neurotrophin factor (CNTF)	Peprotech	Cat# 450-50
Triiodothyronine (T3)	Sigma	Cat# T-2572

(*Continued on next page*)

Continued

REAGENT or RESOURCE	SOURCE	IDENTIFIER
DNase I	Sigma	Cat# D5025
PDGF-AA	Peprotech	Cat# 100-13A
FGF	Peprotech	Cat# 100-18B
TRIzol	Invitrogen	Cat# 15596018
BrdU	Sigma	Cat# B5002
DAPI	Solarbio	Cat# ID2250
Critical commercial assays		
DeadEnd™ Fluorometric TUNEL System kit	Promega	Cat# G2350
ECL kit	ZETA life	Cat# 310231
SurePrint G3 Mouse Gene Expression V2 8×60K Microarray	Agilent	DesignID: 074809
PrimeScript™ RT reagent Kit	Takara	Cat# RR037B
SYBR® Premix Ex Taq™	Takara	Cat# RR420A
Deposited data		
Microarray data	The Gene Expression Omnibus database	GSE178729
Experimental models: Cell lines		
B104 neuroblastoma cell	Nature 249:224-227, 1974	N/A
Experimental models: Organisms/strains		
Mouse: C57BL/6J	Jackson laboratories	Stock No. 000664
Oligonuceltides		
Primer: *Hsp70* Forward: GCCAAACGGTTCATCGGGA Reverse: AGGTGCTATTACCAGCAAGGT	This paper	N/A
Primer: *Hsp40* Forward: CGAGAGGCGGTTCAAGCAG Reverse: CCCCCGAAGAAGTCGAAGG	This paper	N/A
Primer: *Tuj1* Forward: CCCAGCGGCAACTATGTAGG Reverse: CCAGACCGAACACTGTCCA	This paper	N/A
Primer: *Gap43* Forward: TGGTGTCAAGCCGGAAGATAA Reverse: GCTGGTGCATCACCCTTCT	This paper	N/A
Primer: *Homer1* Forward: CTGCTCCTCGGGAAAACGAA Reverse: CGGCACACCACATTGGAATC	This paper	N/A
Primer: *Psd95* Forward: GCTACCAAGATGAAGACACGC Reverse: TTCCGTTCACCTGCAACTCATA	This paper	N/A
Primer: *Syn* Forward: CTCAAAGCCAGCCCCTCC Reverse: AGAGTGGGATGTCAGTCGGA	This paper	N/A
Primer: *Camk2b* Forward: CGTTTCACCGACGAGTACCAG Reverse: GCGTACAATGTTGGAATGCTTC	This paper	N/A
Primer: *Rapgef2* Forward: AAATGGGTGGACATCTAAGGCT Reverse: GCTTTGCTACACGAGTCAACG	This paper	N/A

(*Continued on next page*)

Continued

REAGENT or RESOURCE	SOURCE	IDENTIFIER
Primer: *Nlgn1* Forward: GGTACTTGGCTTCTTGAGCAC Reverse: AAACACAGTGATTCGCAAGGG	This paper	N/A
Primer: *Fmr1* Forward: TGGTGGTGGCATGTAATAACC Reverse: CTTACTGGGGCATAGCATTTGAT	This paper	N/A
Primer: *Ppp1r2* Forward: GTCCGCTATGCTCGCTACAG Reverse: GAATGTGGTCCAAGAAGAGAACA	This paper	N/A
Primer: *Nrxn1* Forward: AACGGACTGATGCTTCACACA Reverse: GATATTGTCACCTGACGCAGATT	This paper	N/A
Primer: *Tas2r1* Forward: CTGCATAGACTGGGTCCAAAG Reverse: GCGATTCTGCTAATTGCCAGAG	This paper	N/A
Primer: *Olfr187* Forward: CATTGTGGGAAACGTCAGTTTG Reverse: GCATCTTTGGGACCACTATGGA	This paper	N/A
Primer: *Svil* Forward: GTCCCAAAGAGACATTCGAGAAA Reverse: CTGTGTGTGTGAACGGTCCT	This paper	N/A
Primer: *Brwd3* Forward: GGACCCTGTAACAAATCCGCT Reverse: CACCTAGTAATGTCTGTACCCCA	This paper	N/A
Primer: *Tnf* Forward: CCCTCACACTCAGATCATCTTCT Reverse: GCTACGACGTGGGCTACAG	This paper	N/A
Primer: *Crx* Forward: GTTCAAGAATCGTAGGGCGAA Reverse: TGAGATGCCCAAAGGATCTGT	This paper	N/A
Software and algorithms		
Clampex 10.0	Molecular Devices	https://www.moleculardevices.com/
Mini Analysis	Synaptosoft Inc	https://www.Synaptosoft.com/
GraphPad Prism 7.0	GraphPad Software	https://www.graphpad.com/
Imaris 9.6.0	Oxford instruments	https://www.imaris.oxinst.com/packages
Bio-Rad CFX manager	Bio-Rad	https://www.bio-rad.com
Feature Extraction software V10.7.1.1	Agilent Technologies	https://www.agilent.com.cn/
ImageJ 1.52p	ImageJ	https://www.imagej.nih.gov/ij
Other		
35 mm confocal culture μ-dishes	IBIDI	Cat#81156

RESOURCE AVAILABILITY

Lead contact

Further information and requests for resources and reagents should be directed to and will be fulfilled by the lead contact, Dr. Wenting Wang (wwt0657@fmmu.edu.cn).

Materials availability

All requests for resources and reagents should be directed to and will be fulfilled by the lead contact, Dr. Wenting Wang (wwt0657@fmmu.edu.cn). This includes selective cell lines and antibodies. All reagents will be made available on request after completion of a Material Transfer Agreement.

Data and code availability

- Data: Data reported in this paper will be shared by the lead contact upon request. The transcriptome profiling datasets are available in the Gene Expression Omnibus database (GSE178729)
- Code: This paper does not report original codes.
- All other items: Any additional information required to reanalyze the data reported in this paper is available from the lead contact upon request

EXPERIMENTAL MODEL AND SUBJECT DETAILS

Primary neuron cultures and irradiation protocol

The animal protocol was approved by the Animal Care and Use Committee of the Fourth Military Medical University. Mouse cortical neurons were prepared as previously reported (Lesuisse and Martin, 2002). Briefly, embryonic day 16 (E16) C57/B6 mice were harvested by cesarean section from anesthetized pregnant dams. Cerebral cortices were isolated and dissociated by trituration with a fire-polished Pasteur pipette. Cultures were plated onto 35 mm confocal culture μ-dishes with polymer coverslip (IBIDI, 81156) at high density (10^5 cells /cm^2) for electrophysiology, RNA extraction and Western blot analyses. Lower density cultures (2×10^4 cells/cm^2) were used for immunocytochemical studies. Tissue culture dishes were coated with poly-D-lysine. The cells were plated in Neurobasal™ Plus Medium (Thermo Fisher, A3582901) supplemented with B27 plus (Thermo Fisher, A3582801), 300 μM glutamine, and Penicillin-Streptomycin. Three days after plating, half of the medium was changed and the medium was changed every 3 days subsequently.

Oligodendrocyte culture and neuron-oligodendrocyte myelinating cocultures

Mouse oligodendrocyte precursor cells (OPCs) were purified as previously reported (Zhao et al., 2014b). Briefly, the mixed glial cells cultured in 60mm dishes were maintained in 10% FBS medium for 5 days to reach ~80% confluence. Then culture medium was replaced with modified OPC growth medium containing B104 neuroblastoma cell conditioned medium (CM) to induce the proliferation of OPCs. Three days later, OPCs reached a yield high enough for isolation and purification. Incubation with DNase I plus EDTA were used to detach the top layer OPCs from the underlying astrocytes. Cell suspensions were then harvested and subjected to differential attachment to eliminate residuary astrocytes. After centrifuge, the single cell suspension was plated into poly-l-ornithine-coated confocal culture dishes with polymer coverslip (IBIDI, 81156), at a density of 3×10^4 cells/cm^2. OPC growth medium (DMEM, insulin 10ug/ul, 1% N2-supplyment) containing 15% B104 CM was used for propagation. To further obtain high purity, OPCs detachment procedure was repeated, and cells were plated either for proliferation or differentiation as mentioned in the manuscript. Both short- and long-term effects were examined as mentioned above. To examine cell proliferation, OPC cultures were maintained in proliferation medium (DMEM/F12, L-Glutamine (4 mM), sodium pyruvate (1 mM), BSA (1 mg/ml), insulin (5 μg/ml), Biotin (10 nM), Apo-Transferrin (50 μg/ml), sodium selenate (30 nM), hydrocortisone (10 nM), penicillin (50 IU/ml), PDGFaa (50 ng/ml) and FGF (10 ng/ml) and irradiated at 1 DIV and 2 DIV, and tested for BrdU incorporation assay at 3 DIV. To study OPC differentiation, cultures were changed to differentiation medium at 1 DIV and irradiated from 2 DIV to 4 DIV. Cultures at 3 DIV, 4 DIV and 5 DIV were fixed for testing OL differentiation.

For OLs/neurons co-cultures, we referred to the method described by Asa and Mazuir (Gardner et al., 2012; Mazuir et al., 2020). The purified OPCs were seeded into dishes with 5 DIV neurons at a density of 4.5×10^5 cells per dish. Then, the medium was changed to coculture medium containing: 1:1 Neurobasal™ Plus Medium with DMEM-high glucose medium (vol), GlutaMAX (1 mM), penicillin-streptomycin (50 IU/ml), sodium pyruvate (1 mM), BSA (1.5 mg/ml), B-27 plus supplement, insulin (10 μg/ml), Biotin (5 nM), Apo-Transferrin (50 μg/ml), sodium selenate (25 nM), NAc (5 μg/ml), CNTF (10 ng/ml), and T3 (15 nM). Co-cultures were maintained for 14 days, with fresh medium half volume changed every 3 days.

METHOD DETAILS

THz irradiation system

Customized quantum cascade laser (QCL) has been introduced in previous study (Zhao et al., 2019) and was driven by CW/QCW bench top current source (IXYS Colorado, PCX-7420). The THz irradiation setup was shown in Figure 1A. The output of the QCL was terminated with an Off Axis parabolic mirror (OPA, Tydex) to get 10 mm wide collimated beam; THz mirror (MR-QC-D50.8-T6.35-C, Tydex) with thickness of gold

coating sufficient to reflect incident THz radiation was used to direct the beam orthogonally to the bottom surface of the culture plate. THz lens (LPX-TPX-D25.4-F50, Tydex) was inserted under the culture dish to focus a collimated beam into defined spot area. The 3A-P-THz sensor (Ophir) measures the CM beam powers in our system, which is sensitive from 15 μW to 3 W. The QCL and all the optical lens are fixed on an optical breadboard.

To calculate the height of culture dish (x) according to the defined spot area (Figure 1C), we used the formula: $x = f - f \cdot r/R$. R is defined as the radius of THz lens (R = 12.7 mm), f is the effective focus length (f = 50 mm), r is the radius of defined spot area (r = 5 mm in our study). The THz power intensity is 70 $\mu W/cm^2$ at the spot area measured by the THz sensor.

Environment controlled THz exposure chamber

A stage top incubator (Olympus, Japan) is placed on an alloy table with aperture and includes three parts to provide 37°C, 5% CO_2 and high humidity condition. First, a stage heater that fits into the aperture of the table insures the stability and exposure spot location of culture dish between repeated irradiations. The viewing aperture is used for THz radiation. Second, condenser aperture cover heater seals the incubator and maintains the inner chamber environment. Third, a circular, heated water tank equipped with carbon dioxide injectors fed by a mixed gas unit (5% CO_2, 95% Air) maintained high humidity.

To measure the temperature rise generated in THz irradiated biological samples, we used digital thermometer (Fluke, 54II B) to record the dish surface temperature during THz exposure in the preliminary experiments. The thermometer with TSU-200F Thermo Probe is connected to D35-200F sensor lid for 35 mm Dishes (Tokai-Hit, Japan). To exclude any external variations in the growth conditions and examine the effect by THz radiation only, control and experimental culture dishes were placed in the center of exposure chamber successively, with or without THz treatment, and processed for further analysis in parallel.

In addition, the whole THz irradiation system and exposure chamber are set in a homemade polymethyl methacrylate box, in which silica gel is used to decrease the environment humidity and permits maximum THz delivery to the biological sample. Two operating windows on the box are designed for placing the sample and adding liquid nitrogen into the QCL.

THz irradiation was delivered to the cultures in short or long duration. For short term effects study, cell cultures were irradiated for 15 minutes (min), 3 times a day, with 3 hours (hr) interval between each irradiation; for long term effects study, cultures were irradiated for 3 hr, one time a day.

Immunocytochemistry and Western blot assay

For immunocytochemistry, cell cultures were fixed in 4% PFA. After TritonX-100 permeabilization for 15 min, samples were incubated with primary antibody for 1 hr at room temperature followed by fluorescent secondary antibody (Millipore) for another hour. The primary antibodies were: mouse anti-Tuj1 (1:1000; R&D systems, MAB1195), rabbit anti-Homer1 (1:500; abcam, ab184955), mouse anti-CNPase (1:500; Biolegend, 836404), rat anti-MBP (1:1000; Abcam, ab7349), rabbit anti-PDGFRα (1:500; BD Pharmingen, 558774), rabbit anti-Olig2 (1:200; Millipore, AB9610). Cells were then counter-stained with DAPI (1ug/ml; Solarbio, ID2250) and visualized with Olympus FV 1000 Confocal microscope. Experiments were replicated using cells from three different primary cultures.

For BrdU pulse labeling, cultures were incubated with BrdU (10 μM, sigma, B5002) 4 hr prior to fixation. For the staining of BrdU, before permeabilization, culture samples were subjected to DNA denaturation with 2N hydrochloric acid at 37°C for 10 min and then neutralized with 0.1 M sodium borate at pH 8.5 for 2 X 10 min. The G3G4 monoclonal antibody (anti BrdUrd, 1:40, G3G4) was obtained from the Developmental Studies Hybridoma Bank developed under the auspices of the NICHD and maintained by The University of Iowa.

For apoptosis analysis, neurons were subjected to DeadEnd™ Fluorometric TUNEL System kit (Promega, G2350) as introduced in product information.

For Western blot analysis, protein lysates were resolved by SDS–PAGE and blotted using standard procedures. Antibodies used were rabbit anti Synaptophysin (1:1000, abcam, ab32127), mouse anti β-actin

(1:20000, Sigma, A2228), and horseradish peroxidase–conjugated secondary antibodies (1:10000, Abbkine). Signals were revealed by chemiluminescence with the ECL kit (ZETA, 310231), according to the manufacturer's instruction.

Electrophysiological recording

The dish was placed on the stage of upright microscope (BX-51WI, Olympus, Japan) and constantly perfused with carbongenated ACSF at 24–28°C (TC-324B, Warner Instruments). Whole-cell patch clamp recordings were performed with IR-DIC visualized guide. Patch pipettes (BF150-86-7.5, Sutter Instruments, USA) were pulled in a horizontal pipette puller (P-97, Sutter Instruments, USA) with a tip resistance of 3–5 MΩ. For the intrinsic properties recording, the pipettes were filled with the solution containing (in mM): 128 potassium gluconate, 10 HEPEs, 10 phosphocreatine sodium salt, 1.1 EGTA, 5 ATP magnesium salt, 0.4 GTP sodium salt. pH was adjusted to 7.3 with KOH, and osmolarity was adjusted to 300–305 mOsm with sucrose. For the spontaneous excitatory postsynaptic currents (sEPSCs) recording, the internal solution of the pipettes contained (in mM): 120 CsMeSO3, 5 NaCl, 4 NaCl, 10 TEA-Cl, 10 HEPES, 0.1 EGTA, 4 lidocaine N-ethyl chloride, 4 ATP magnesium salt, and 0.3 GTP sodium salt. pH was adjusted to 7.2–7.4 with CsOH, and osmolarity was adjusted to 298–300 mOsm with sucrose. Cells with series resistance more than 20 MΩ at any time during the recordings were discarded. Liquid junction potentials were not corrected.

A MultiClamp 700B amplifier (Molecular Devices, USA) was used to recording either currents or membrane potential. Signals were low-pass filtered at 5 kHz and sampled at 20 kHz with a Digidata 1550B and Clampex 10.0 (Molecular Devices), and data were stored on a computer for subsequent off-line analysis. During the sEPSCs recording, the cell membrane potential was clamped at −70 mV in the presence of 25 μM BMR (1(S),9(R)-(−)-bicuculline methobromide) (Selleckchem, USA). The sEPSCs were detected and analyzed using Mini Analysis (Synaptosoft Inc., USA). During the recording of the neurons' intrinsic properties, the resting membrane potential more negative than – 40 mV and action potentials with overshooting were selected for further experiments.

RNA extraction, qRT-PCR and microarray assay

Total RNAs were purified from cell cultures using TRIzol reagent according to the manufacturer's instruction (Invitrogen). RNA concentrations were measured with NanoDrop ND-2000 spectrophotometer (Thermo Scientific), and the quality (RNA Integrity Number, RIN) was assessed using the Agilent 2100 Bioanalyzer system (Agilent Biotechnologies). RNA was transcribed to cDNA with the PrimeScript™ RT reagent Kit (Perfect Real Time, Takara) and reactions were performed with SYBR® Premix Ex Taq™ (Takara) in CFX96 Touch Real-Time PCR Detection System (Bio-Rad). Relative gene expression was normalized to internal control β-actin.

Microarray analyses service was provided by OE Biotechnology Co., Ltd. (Shanghai, China). For each sample, 250 ng of total RNA from either control or THz samples was used to prepare Cy3 labeled fragmented cRNA for analysis on Agilent SurePrint G3 Mouse Gene Expression V2 8×60K Microarray (DesignID: 074809). Sample preparation, processing, and hybridization were conducted according to the technical manual. The arrays were finally scanned using Agilent Scanner G2505C and Feature Extraction software (V10.7.1.1, Agilent Technologies) was used to analyze array images to get raw data. Next, the raw data was normalized with the quantile algorithm. Differentially expressed genes were then identified through fold change as well as P value calculated with t-test. Only genes exhibiting at least a two-fold expression difference with $p < 0.05$ in all pairs of samples were considered to be differentially expressed and subsequently used for GO and KEGG pathway analysis. Hierarchical Clustering was performed to display the distinguishable genes' expression pattern among samples. The transcriptome profiling dataset have been deposited in the Gene Expression Omnibus database (GSE178729). To further confirm the microarray results, we perform qRT-PCR for selected genes. Primer sequences for SybrGreen probes of target genes are listed in Star Methods table.

QUANTIFICATION AND STATISTICAL ANALYSIS

All statistical analyses were performed in Prism 7.0 (GraphPad Software, Inc., USA). Values were expressed as Means ± SEM. The details of the statistical methods were mentioned in the text or figure legends. All data were obtained by counterbalancing experimental conditions with controls. Statistical significance was accepted when $p < 0.05$.